

RESEARCH

Open Access



Effect of the Curing Condition and High-Temperature Exposure on Ground-Granulated Blast-Furnace Slag Cement Concrete

Eskinder Desta Shumuye¹, Jun Zhao^{1*}  and Zike Wang²

Abstract

In this study, the effect of curing temperature on the properties of slag cement concrete after high-temperature exposure was studied, and elevated curing temperature (45 ± 2 °C and 95% relative humidity (RH)) was selected to compare with the standard curing temperature (20 ± 2 °C and 95%RH). Four different concrete mixes with the same mix proportion, except for different slag replacement ratios, were used: 0% (reference), 30% (slag), 50% (slag), and 70% (slag). After high-temperature exposure at 200, 400, 600, and 800 °C, the effect of slag replacement, high temperature, and curing temperature on the compressive strength and mineralogical and microstructural properties of slag cement concrete were studied. Test results indicated that the compressive strength of concrete cured for 7 d at elevated temperatures increased by 28.2, 20.7, 28.8, and 14.7% compared with that cured at the standard curing condition at slag percentages of 0, 70, 50, and 30%, respectively. X-ray diffraction (XRD) and Scanning electron microscope (SEM) results revealed that concrete cured at elevated temperatures exhibited a more condensed phase and contained a higher percentage of hydrates than that cured for 7 d in the standard curing condition. However, after 56 d of curing, concrete in the standard curing condition exhibited a more stable phase and a higher concentration of hydrates.

Keywords: concrete, compressive strength, curing condition, high-temperature, microstructure, slag

1 Introduction

Fire is highly hazardous to buildings and structures. Industrial waste materials, such as ground-granulated blast-furnace slag (GGBS), have been used to produce blended cement. These blended cements are widely used as construction materials or for the maintenance of concrete structure, e.g., remediating cracks in bridge joints and roadways (El-Yamany et al. 2018).

The effect of high-temperature exposure on the behavior of slag-blended cement materials has been

investigated scientifically (Aldea et al. 2000a; Bakharev et al. 1999; Behfarnia and Shahbaz 2018; Netinger et al. 2013; Shumuye et al. 2019) and results have been affirmative. It has been reported (Bakharev et al. 1999; Chini 2005; Jung and Choi 2017; Li and Hu 2014; Wang 2008) that, concrete comprising granulated blast-furnace slag (GGBFS) cement exhibits an earlier strength development under elevated curing temperature owing to the temperature-dependent properties of slag cement.

Substantial literature is available regarding the application of supplementary cementitious materials in concrete; however, studies regarding the effect of elevated curing temperature on the strength development of concrete containing high-volume supplementary cementitious materials are rare (Aldea et al. 2000a; Jung and Choi

*Correspondence: zhaoj@zzu.edu.cn

¹ School of Civil Engineering, Zhengzhou University, Zhengzhou 450001, China

Full list of author information is available at the end of the article
Journal information: ISSN 1976-0485 / eISSN 2234-1315

2017; Li and Hu 2014; Wang 2008). Jung and Choi (2017) investigated the effect of elevated curing temperature on the compressive strength development of concrete containing high volumes of GGBS. The test results indicated that after 28 days, the compressive strength development of concrete cured at elevated temperature of 65 °C was significantly affected, being about 10–18% higher than the samples cured at elevated temperature of 55 and 75 °C (Jung and Choi 2017).

Wang et al. (2014) studied the effect of elevated curing temperature on the compressive strength of high-volume slag cement, indicating that the activity of ground iron and steel slag is more sensitive to the increase in curing temperature than that of OPC. Kim (2010) reported that increasing the curing temperature before 7 d significantly affected the strength improvement at a later age.

Furthermore, researchers (Akca and Özyurt 2018; Guerrieri and Sanjayan 2009; Long et al. 2019; Mendes et al. 2009) have studied the performance of concrete specimens under different levels of high-temperature exposure to determine the effects of temperature on the microstructure and physico-mechanical properties of slag cement concrete. According to (Akca and Özyurt 2018; Guerrieri and Sanjayan 2009), the mechanical properties of concrete decreased considerably after a high-temperature exposure because the initial morphology of concrete changed after high-temperature exposure. (Mendes et al. 2009) reported that the first weight loss occurred between 100 and 200 °C owing to the loss of capillary water, and that further weight loss occurred when the exposure temperature increased to 400–600 °C because of the dehydration of Ca(OH)₂. When the high-temperature exposure exceeded 800 °C, weight loss owing to CaCO₃ decarbonation occurred.

However, the effect of elevated curing temperature on the microstructural and mechanical properties of slag cement concrete under high-temperature exposure is still ambiguous. The objective of this study is to assess and analyze the mechanical, physical, and microstructural properties of GGBS cement concrete exposed to high temperatures in normal and elevated curing temperature conditions.

2 Materials and Mix Design

2.1 Materials

OPC-labeled (P.O42.5) and GGBS-labeled S95, conforming to the Chinese standard specifications (GB175 and GB/T18046) (China Building Materials Science Research Institute 2007) were used. Natural well-graded river sand and granite with a maximum nominal size of 20 mm were used as fine and coarse aggregates, respectively. Table 1 displays the mineralogical composition and specific gravities of OPC and GGBS cement.

Table 1 Chemical composition and specific gravity of cement and GGBS (%wt.).

Component (%)	OPC	GGBS cement
SiO ₂	17.945	26.713
Al ₂ O ₃	4.465	14.748
Fe ₂ O ₃	3.558	0.472
CaO	64.562	43.093
MgO	3.751	10.145
Rb ₂ O	0.005	0.000
Na ₂ O	0.178	0.380
K ₂ O	1.176	0.346
MnO	0.059	0.260
TiO ₂	0.261	0.662
P ₂ O ₅	0.064	0.010
NiO	0.005	0.003
ZnO	0.060	0.000
Specific gravity	3.15	2.89

Table 2 Mix proportions of concretes per cubic meter.

Materials	Mixture designation			
	G-70	G-50	G-30	G-0
OPC (kg)	129.3	215.5	301.7	431
GGBS cement (kg)	301.7	215.5	129.3	–
Water (kg)	202.7	202.7	202.7	202.7
w/cm	0.47	0.47	0.47	0.47
Coarse aggregates (kg)	1052.6	1052.6	1052.6	1052.6
Fine aggregates (kg)	755.2	755.2	755.2	755.2

2.2 Mix Design

One reference concrete mix without GGBS cement (G-0) and three concrete mixes incorporating GGBS cement were prepared with 30% GGBS (G-30), 50% GGBS (G-50), and 70% GGBS (G-70), as shown in Table 2. After some trial mixes, the total content of cementitious materials and water/cementitious material ratio (w/cm) were set as 431 kg/m³ and 0.47, respectively.

3 Experimental Process

3.1 Mixing

The concrete mixtures were mixed using a revolving drum pan mixer of 60-L capacity. Proper homogenous mixing was ensured by continuously mixing for 5–6 min. After that the mixture was poured into 150 × 150 × 150 mm plastic molds. The specimens were then vibrated using a vibrating table for 2 min to release any entrained air and allowed to set for 24 h and then taken to the specified curing condition.

3.2 Curing Condition of Specimens

All specimens were demolded after 24 h. Subsequently, concrete specimens were obtained at two different curing regimes, as follows:

- Ambient curing: the samples were stored in the laboratory environment for 24 h. Subsequently, the samples were de-molded and stored in the standard curing condition at a constant temperature of 20 ± 2 °C, complying with (ASTM C09 Committee 2001a) and 95% relative humidity (RH) for 7, 28, and 56 d.
- Elevated curing temperature: the samples were stored in the laboratory environment for 24 h. Subsequently, the samples were demolded and cured in an elevated curing temperature chamber at a constant temperature of 45 ± 2 °C at approximately $95 \pm 2\%$ RH for the first 7 d. Next, the samples were stored in the standard curing condition at a constant temperature of 20 ± 2 °C and $95 \pm 2\%$ RH until testing was commenced.

All concrete specimens were stored in two different curing environments, as specified above. For each test, all reported results were the average of three measurements. Among 450 concrete specimens, 432 were exposed to each of the four maximum exposure temperatures (200, 400, 600, and 800 °C) for three different exposure durations. For all concrete mix groups, nine concrete cubes, which were cured in the two curing environments above, were tested at ambient temperature exposure.

3.3 Testing Methods

3.3.1 Compressive Strength

The compressive strength of concrete cured at both in elevated curing temperature and standard curing conditions were measured on the cube specimens ($150 \times 150 \times 150$ mm) using a 3,000 kN testing machine according to, (ASTM International 2001). The strength measurements of concrete were performed at the ages of 7, 28, and 56 d, and the average of three measured values was reported complying with the (RILEM Technical Committee 200-HTC 2007a). The specimens were loaded to failure after being cooled at room temperature.

3.3.2 Mass Loss

The concrete mass loss was obtained by recording the average test result of three concrete specimens for each fire exposure. The specimens were weighed before and after each heating to determine the mass loss quantity of concrete during the fire exposure, complying with the (RILEM Technical Committee 200-HTC 2007b).

3.3.3 Scanning Electron Microscopy (SEM)

To study the morphology of the samples, SEM images were obtained using a scanning electron microscope. The samples were split to a suitable size immediately before observation by the process of splitting the specimens freshly to avoid surface carbonation. Additional preparation of the samples was made by coating the sample's surface with ejection of gold/palladium (Au/Pd) under high vacuum conditions (Shumuye et al. 2019). In this process, the acceleration voltage of 20 kV was used. The actual magnification of the images was printed on the SEM pictures.

3.3.4 X-ray Diffraction (XRD)

After the specimens were subjected to a compressive strength test, crushed mortar powder was used for XRD test to examine changes in the hydration products for each replacement percentage (Ukpatha et al. 2019). Results from the XRD test of the concrete samples were used to identify the crystalline phase of the dehydration process after high-temperature exposure.

3.3.5 Ambient Temperature

At 7, 28, and 56 d, the specimens were subjected to temperatures of 200, 400, 600, and 800 °C for different exposure times using a computer-controlled furnace powered by gas and electricity. An in-built thermocouple in the furnace enabled its temperature to be recorded throughout the test.

Hitherto, the heating rates employed by researchers differ, which vary between 0.5 °C/min and the ISO-834 standard fire curve (Arioz 2007; Chan et al. 1999; Gencel 2012; ISO 834-1-1999, 1999; Vieira et al. 2011; Yang et al. 2018; Yu et al. 2015; Zhao et al. 2017). Related studies show that the heating rate ranging from 1 to 10 °C/min marginally affected the residual strength of concrete (Shumuye et al. 2019; Yang et al. 2018; Zhang et al. 2000; Zhao et al. 2017). The reason for applying slow heating rate for 200 and 400 °C is practically using the electronic gas furnace is not safe to extract samples from the furnace during the test. Since the temperature inside the furnace will reach 200 and 400 °C within 1 and 1.5 min when we follow ISO 834 standard, respectively, whereas by using 10 °C/min heating rate we can attain the target temperature within 23 and 37 min starting from the ignition, and this time duration will allow us to control our gas supply during the exposure time for a possible sample extraction by following appropriate safety procedure. Furthermore, when we compare the specimens with control specimen, the temperature and heating rate are the same.

After attaining the target temperature, the first group of concrete was removed and allowed to cool at 21 ± 2 °C. To achieve a thermal steady state (such that the inner core of the concrete specimen is approximately the target temperature) (Yang et al. 2018; Zhao et al. 2017), the other concrete specimens of the group were retained at the same temperature for 1 and 2 h Fig. 1.

4 Results and Discussion

4.1 Compressive Strength

Results of compressive strength test for all concrete mixes in the two curing conditions are shown in Table 3 and Fig. 2. The results in Table 3 are presented as values in MPa and as the relative compressive strength compared with the reference concrete. As shown in Table 3, the compressive strength of concrete cured at elevated temperature is higher than that cured in the standard curing condition at 7 d. In addition, the compressive

strength increased with the curing time for all concrete groups for both curing conditions. Figure 2 shows that using a 30% slag replacement yielded a lower compressive strength for both curing conditions, whereas 50% slag replacement is considered the optimal compressive strength for both standard and elevated curing temperature conditions. Concrete specimens with 50% and 70% slag replacement exhibited similar values of compressive strength compared with the reference specimens. The compressive strength of concrete increased significantly between 7 and 28 d in the standard curing condition; however, the result became almost steady for concrete cured at elevated temperature.

Based on the data provided in Fig. 2, it is clear that the compressive strength at 7 d in the elevated curing temperature condition for concrete groups G-0, G-30, G-50, and G-70 increased by 28.2, 20.7, 28.8, and 14.7%, respectively, compared with that at the normal curing condition. This result encourages the use of slag cement

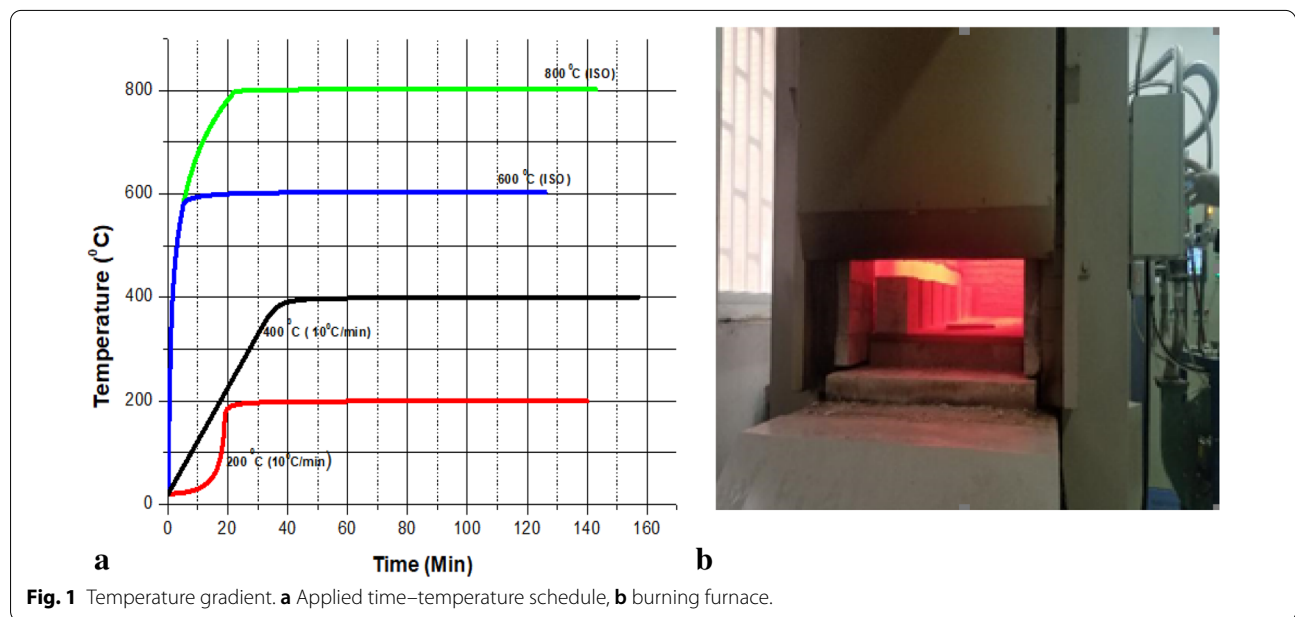


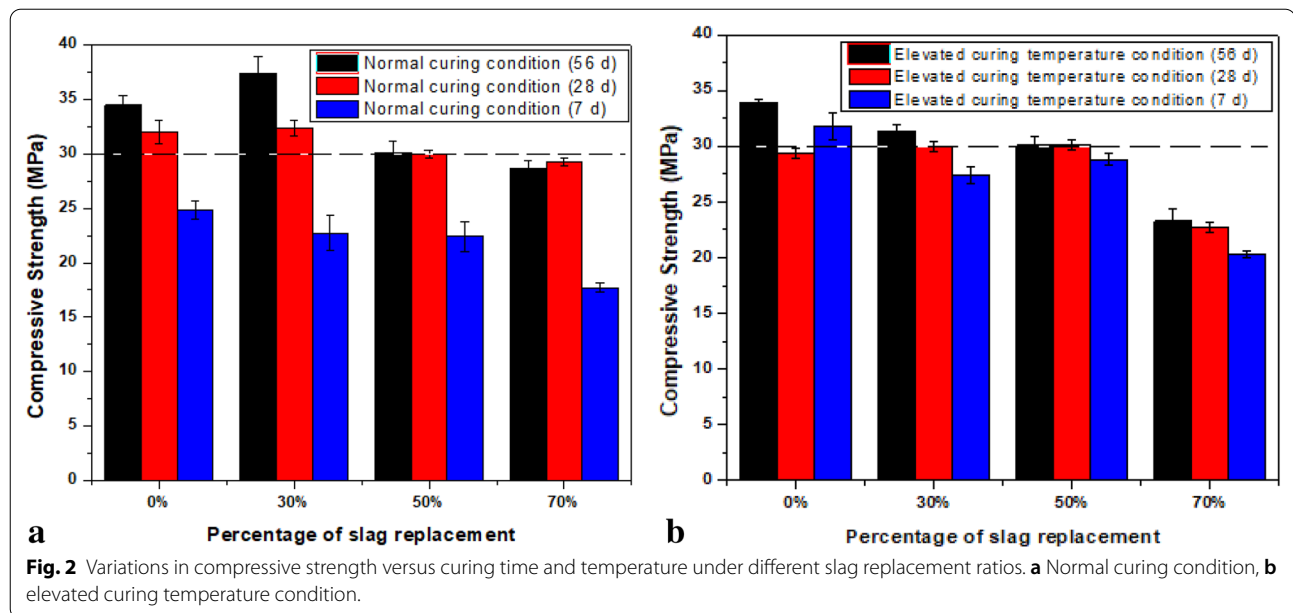
Fig. 1 Temperature gradient. a Applied time-temperature schedule, b burning furnace.

Table 3 Variation in compressive strength vs. curing time and temperature under different slag replacement ratios.

Curing time (day)	Mix code											
	RC (G-0)			G-30			G-50			G-70		
	MPa			MPa			MPa			MPa		
	NT.C	ET.C	%	N.C	ET.C	%	N.C	ET.C	%	N.C	ET.C	%
7	24.8	31.8	28.2	22.7	27.4	20.7	22.4	28.8	28.6	17.7	20.3	14.7
28	32.0	29.4	- 8.1	32.4	30.0	- 7.4	30.0	30.1	0.3	29.2	22.7	- 22.2
56	34.5	33.9	- 1.7	37.4	31.4	- 16.0	30.9	30.1	-2.6	28.7	23.3	- 23.1

NT.C normal temperature curing.

ET.C elevated curing temperature.



in hot climate regions as a considerable loss in ultimate compressive strength is unlikely. However, as shown in Table 3, for the concrete at 28 and 56 d, variations in compressive strength became negative compared with the control concrete group for both curing conditions. After achieving higher compressive strengths at early ages, the compressive strengths of concrete began to decrease at later ages for concrete specimens cured at elevated temperature. This test results demonstrate that elevated temperature curing might result in an advantageous high early strength development, but a disadvantageous long-term strength development. A prior study stated that heat curing seems to have unpleasant influence on strength development, particularly at later ages (Barnett et al. 2006; Jung and Choi 2017). Furthermore, under an elevated temperature curing, the water loss rate of concrete is faster, which leads to more porosity in the concrete structure and significantly influences its strength. (Tang et al. 2017) also explained that the reason for the relaxation of strength development rate once the curing time exceeds 7 days. This is because, exposure in elevated curing temperature is favorable to speed up the rate of the hydration reaction of cement. Promoting this reaction, results in a rapid strength development over the initial curing time. The formation of C–S–H gels exhibiting needle-like structures at the early ages delays the subsequent hydration process owing to the reduction in compressive strength at the later age due to more porous and less cohesive structures in the concrete compared with concrete cured in the standard curing condition, as confirmed by the XRD test; similar results were have been reported by (Çakır and Aköz 2008). On a prolonged

curing condition for 56 d, concrete specimens cured at 45 ± 2 °C did not exhibit better compressive strength results than those cured at 21 ± 2 °C. This may be attributed to the reactivity of the slag at 45 ± 2 °C. Only a slight change occurred in the hydration of slag cement concrete at 21 ± 2 °C and 45 ± 2 °C at 28 and 56 d. This indicated that a prolonged curing condition at low curing temperatures was more beneficial for the microstructure development of slag-blended concrete. The hydration of the slag mixtures increased slightly with increased temperature. Meanwhile, (Ukpata et al. 2019) reported a slight decrease in the degree of slag hydration with increasing replacement.

It was observed that the 7-d compressive strength of concrete groups G-0, G-30, G-50, and G-70 were 71.8%, 60.6%, 72.4%, and 61.6% of their 56-d compressive strength, respectively, for concrete specimens cured at the standard curing condition. Meanwhile, for concrete specimens cured at elevated temperature, the 7-d compressive strength of concrete groups G-0, G-30, G-50, and G-70 were 93.8%, 87.2%, 95.6%, and 87.1% of their 56-d compressive strengths, respectively. Furthermore, the 28-d compressive strength of concrete groups G-0, G-30, G-50, and G-70 were 92.7, 86.6, 97.0 and 79.0% of their 56-d compressive strengths, respectively. For concrete specimens cured at elevated temperature, their 28-d compressive strengths were 86.7, 95.5, 100 and 97.4% of their 56-d compressive strengths, respectively. Comparing all the results listed above and the strength development after the age of 28 d is insignificant. The compressive strengths for concrete groups G-30 and G-50 at 28 d was similar to that of concrete

group G-0 and its strength reached the highest value at 56 d. According to (Cho et al. 2017), the highest strength attained in the longer term curing was attributed to the latent hydraulic properties of slag cement.

4.2 Fire Resistance of Concrete

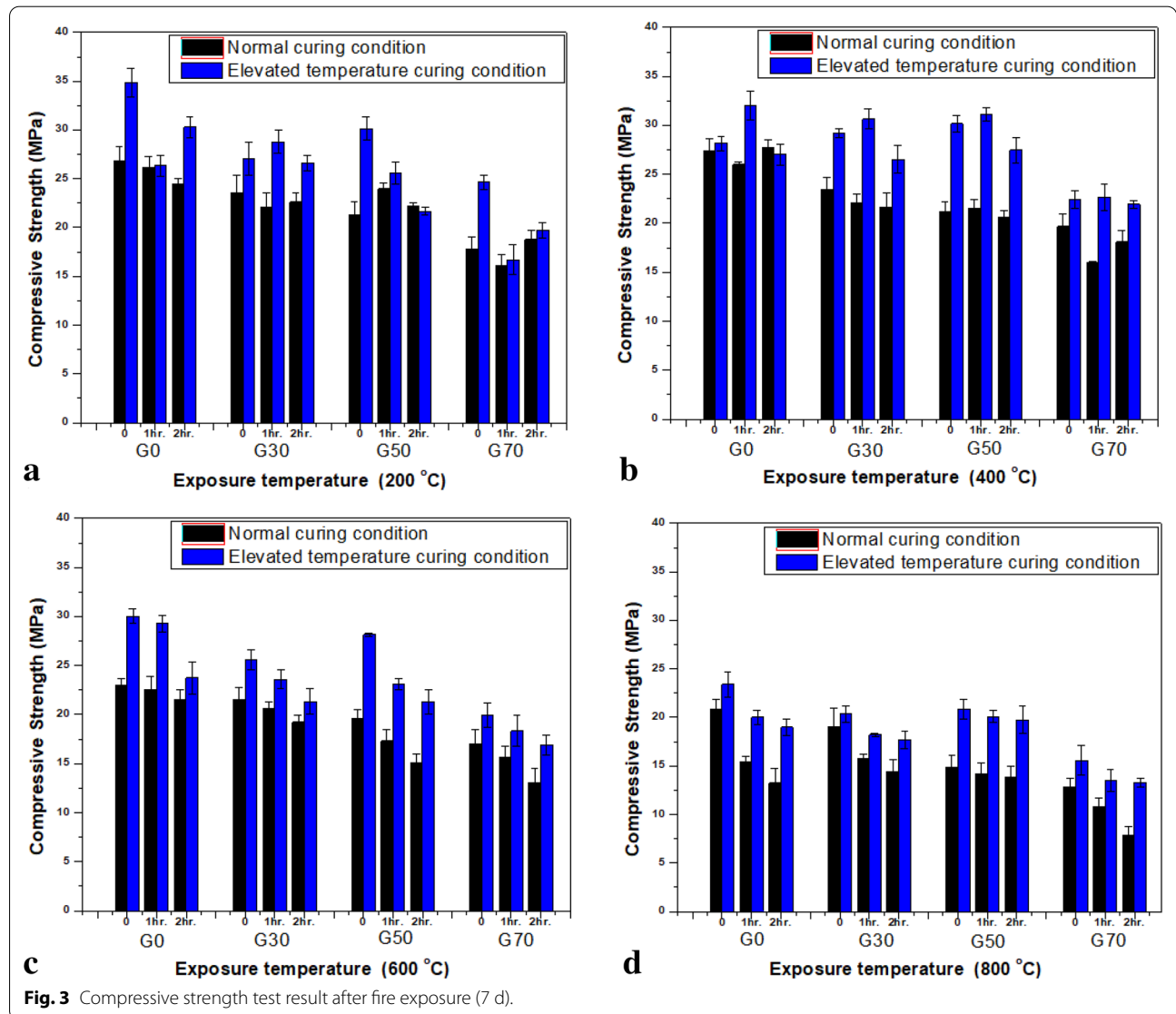
The high-temperature resistance of the concrete mixture was estimated to verify the effect of high temperature on the concrete specimens. The residual value of each concrete property is discussed.

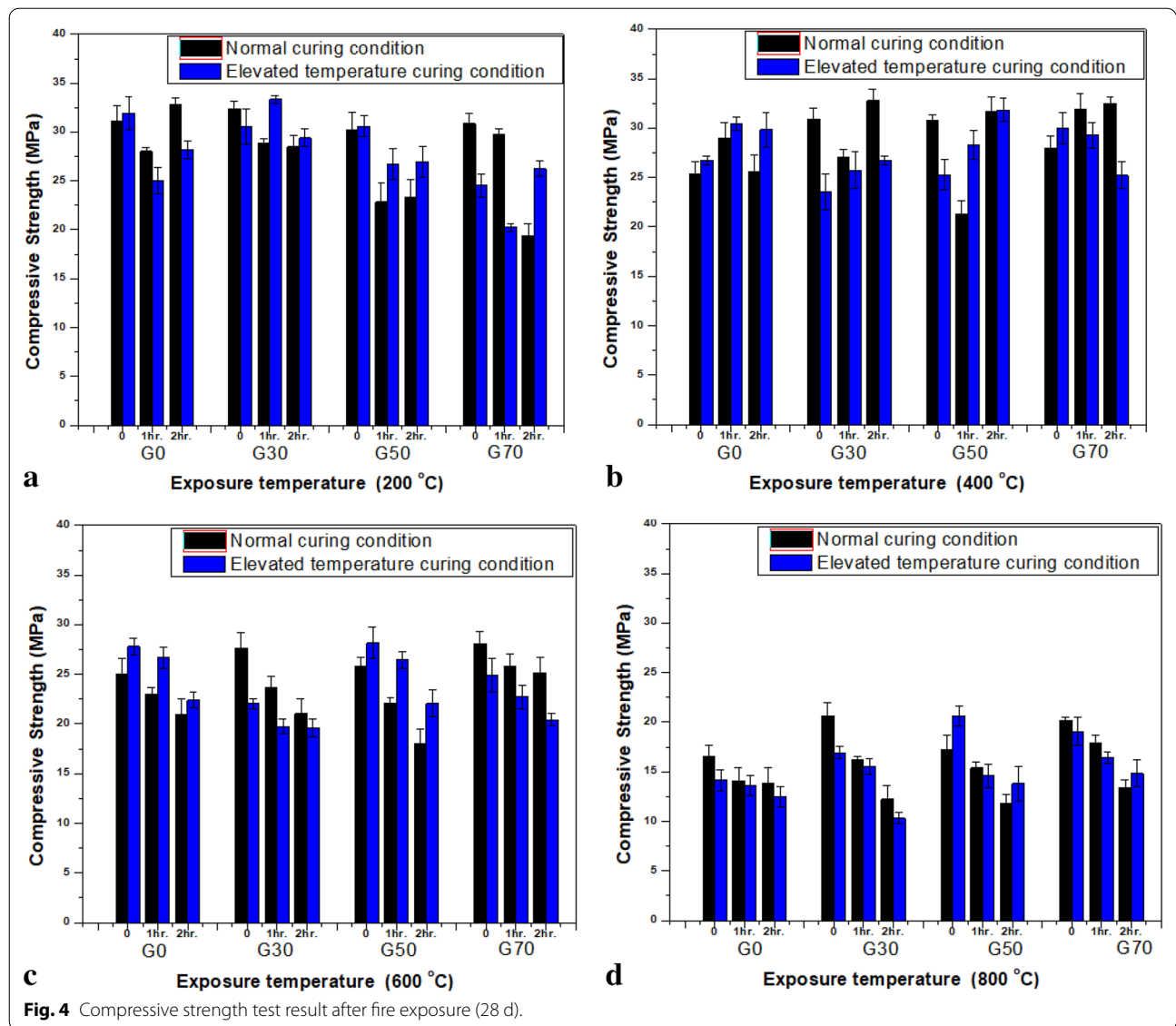
4.2.1 Residual Compressive Strength

The compressive strengths of the specimens were studied after an elevated temperature exposure, and the percentages of residual strengths were calculated relative to the

respective reference concrete samples. The variations in residual compressive strengths of specimens G-0, G-30, G-50, and G-70 under the two curing conditions are plotted in Figs. 3, 4, 5.

As shown in Figs. 3, 4, 5, the residual compressive strengths of the concrete cured at the standard curing condition fluctuated initially with an increase until the temperature reached 400 °C owing to an additional hydration of unhydrated products, termed the “dry hardening” phenomenon by (Khan et al. 2013), thereby increasing the strength resulting from the further hydration of binders and possible development of C–S–H. All concrete mix groups in the elevated curing temperature condition indicated a strength fluctuation at 200 °C exposure. (Türker et al. 2016) reported

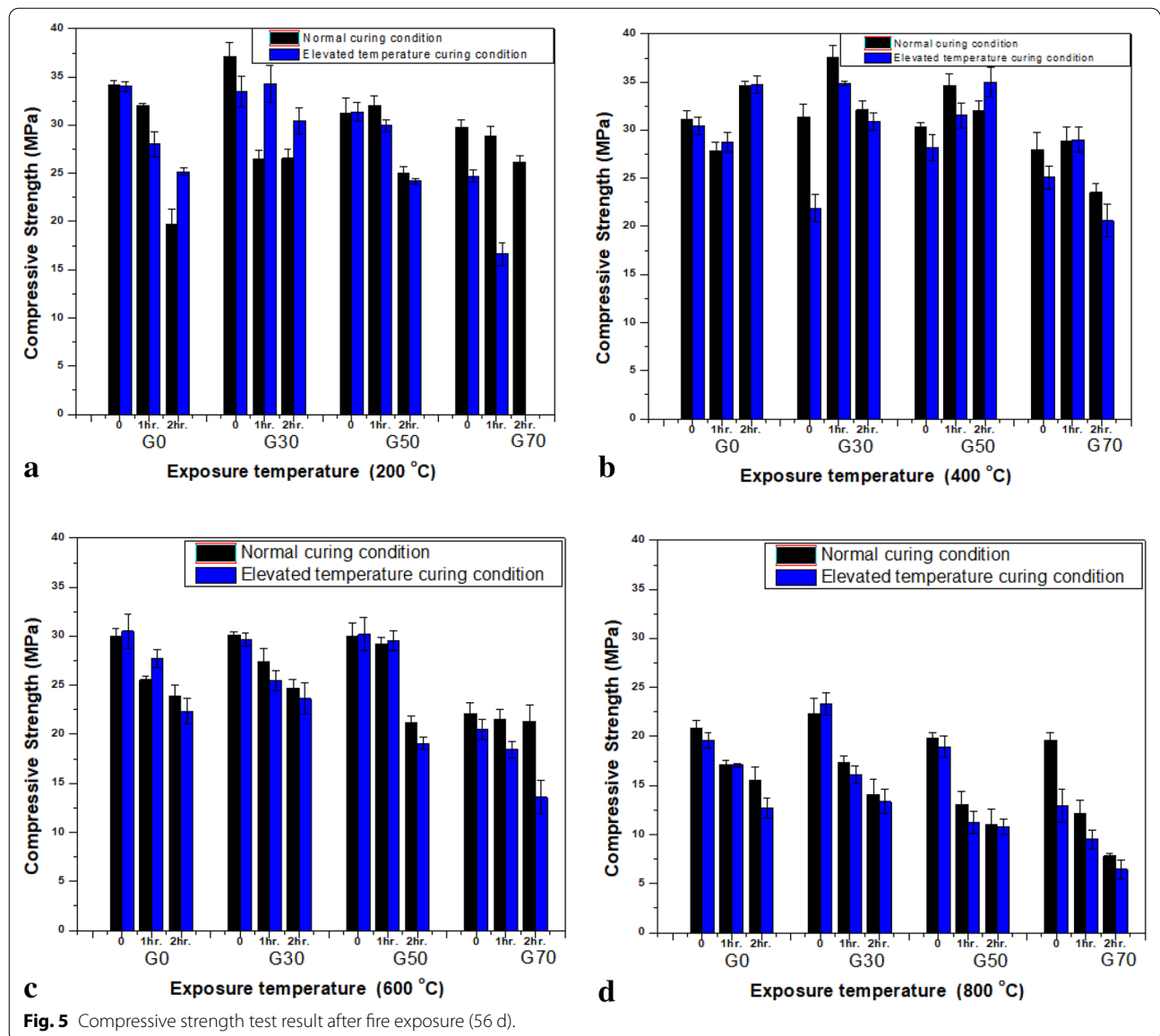




a decrease in the residual compressive strength of concrete containing slag cement subjected to high temperatures of up to 200 °C. However, a few researchers have reported an increase in residual compressive strength with high-temperature exposure ranging from 200 to 400 °C owing to the hydration of unhydrated cement grains in the microstructure (Lublóy et al. 2017). However, with a further increase in the peak temperature and exposure duration, the residual compressive strength decreased significantly. (Mohammad Hosseini et al. 2018) and (Durgun and Sevinç 2019) tested slag cement concrete in a high-temperature exposure range of 400–800 °C and observed a decrease in the strength of concrete residual compressive strength with an increase in high-temperature exposure.

The residual compressive strengths of all concrete mixes cured at the standard curing condition decreased compared with their control group when the high-temperature exposure increased to 600 and 800 °C. However, for concrete cured at elevated temperature, the residual compressive strength reduced compared with its control group exposed at 400, 600, and 800 °C for all concrete mix groups. The residual compressive strength loss related to the increase in high-temperature exposure could be due to moisture loss during heating.

Figure 4 shows the data of all concrete mixes, including an initial compressive strength versus residual compressive strength plot at 28-d curing. Concrete groups G-0, G-70, G-50, and G-30, with relatively high initial compressive strengths, experienced an increase in residual



compressive strength at 200 °C exposure compared with its unexposed control concrete specimens up to 8.6%, 1.6%, 8.1%, and 1.9%, respectively, in elevated curing temperature conditions. Meanwhile, when the exposure duration was extended to 1 h, the loss in residual compressive strength increased for all concrete groups except for the concrete group with a high slag content (G-70). As the exposure duration prolonged to 2 h, the loss in residual compressive strength increased. Meanwhile, for concrete cured at the standard curing condition, all concrete groups except concrete group G-0 lost its residual compressive strength after 2 h of exposure. Hence, the effect of elevated curing temperature is more pronounced for high-volume slag concrete groups.

Furthermore, Fig. 4 shows that for a given high-temperature exposure, the residual compressive strengths of the specimens decreased with an increase in slag content. However, the decrease in residual compressive strength with an increase in high-temperature exposure was significant in the case of concrete cured at elevated temperature, compared with that of specimens cured at the standard curing condition.

At 56-d, the residual compressive strength of G50 and G70 concrete groups are 13.01 and 12.18% lower than that of G0 control concrete mix, respectively, under normal curing condition at 600 °C high-temperature exposure for 2 h duration, while concrete group G30 shows a slight increment (3.16%) in strength compared to the

control mix. It can be also seen from Fig. 5 that concrete groups G30, G50 and G70 have shown 9.59, 41.19, and 97.33% strength reduction compared to G0 control mix, respectively, at 800 °C exposure temperature. The 56-d residual compressive strength under normal curing for concrete groups G0 and G30 shows almost the same trend; the strength reduced by 44.19 and 51.52% compared to its unexposed concrete groups, respectively, at 600 °C exposure temperature. Likewise, concrete group G50 and G70 also faced a 181.9 and 266.0% strength reduction, respectively, at 800 °C exposure temperature.

It was observed that, for all concrete groups preserved at elevated temperature curing a lower residual strength was recorded after 800 °C exposure temperature for 2 h compared to samples cured at normal temperature. The residual strength reduction of G0, G30, G50 and G70 concrete groups are 21.7, 5.61, 1.2 and 21.7% than the same concrete group cured in normal curing temperature at 56d, respectively. Under elevated temperature curing, concrete groups G50 and G70 have experienced a 17.4 and 97.3% strength reduction than that of G0 control concrete mix, respectively, at 800 °C exposure temperature. Notwithstanding, concrete group G30 shows a slight increment (4.89 and 5.5%) in strength same as in normal temperature curing conditions, compared to the control mix at 600 °C and 800 °C exposure temperature, respectively. The strength reduction under 800 °C exposure, for concrete groups G0, G30, G50 and G70 are 166.6, 134.8, 177.9 and 261.6% compared to samples without high-temperature exposure, respectively. Meanwhile, the percentage of strength reduction shows cut-back as the high-temperature exposure reduced to 600 °C for all concrete groups.

4.2.2 Mass Loss of Specimens

The mass loss of the concrete specimens owing to fire exposure was evaluated by measuring the mass of the concrete specimens before and after fire exposure. The percentages of mass change at different temperatures were calculated. The percentages of mass loss of the concrete specimens owing to fire at 28 d are shown in Fig. 6.

As shown in Fig. 6, all specimens revealed a significant mass loss after 1 and 2 h of fire exposure to 200 °C. Subsequently, the percentage mass loss increased at a lower rate at 400 and 600 °C fire exposure. Furthermore, the percentage mass loss increased again at a higher rate at 800 °C fire exposure because of the spalling of the specimens.

The effect of high temperature can be categorized into three different temperature phases, in accordance with the difference in the residual mass of concrete specimens obtained at high temperatures. In the first phase, owing to the evaporation of free water in concrete, the

percentage mass loss was insignificant for all concrete groups. In the second phase, the temperature exposure was increased to 200–400 °C, and the percentage mass loss increased more compared with the first phase owing to the additional evaporation of chemically bonded water; similar results have been reported by (Georgali and Tsakiridis 2005; Shumuye et al. 2019; Yermak et al. 2017).

In general, when the exposure duration was extended to 1 and 2 h at every high-temperature exposure, the percentage mass loss was upstretched gradually with the exposure duration. Furthermore, the mass loss increased with the exposure period regardless of the heating temperature. The average mass loss for the concrete specimens cured in the standard curing condition was 2.64% at 200 °C for an exposure period of 140 min, whereas at 400, 600, and 800 °C, the average mass loss owing to fire exposure for 157, 126, and 143 min exposure was 7.06%, 8.02%, and 9.93%, respectively, which indicated a significant trend change with the change in temperature. For concrete specimens cured at elevated temperature, the average mass loss was 2.09% at 200 °C for an exposure period of 140 min, whereas at 400, 600, and 800 °C, the average mass loss owing to fire for 157, 126, and 143 min exposure was 5.59%, 6.8%, and 8.83%, respectively. Comparing the two curing conditions, the percentage mass loss was more significant for concrete cured at standard curing conditions than that cured at elevated temperature.

4.2.3 Visual Inspections

Photographs of the specimens after exposure at 200, 400, 600, and 800 °C are shown in Figs. 8, 9, 10. These pictures clearly indicate the effect of slag replacement on the amount of surface cracking of the specimens after high-temperature exposure. As the ambient temperature increased, chemical and physical transformations occurred at a high speed. Beyond 100 °C, physically bound water was released. Furthermore, beyond 300 and 500 °C, the silicate hydrate phase decomposed and the Portlandite dehydrated, respectively (Albrektsson et al. 2011).

When the exposure duration and temperature increased to beyond 800 °C for 1 h, changes in the concrete volume became evident, aggregates started to expand and undergo crystalline changes. In addition to the previously discussed strength reduction, all concrete specimens exhibited cracks, spalling, and change in color. The variation in color change was primarily dependent on the aggregate type (Lau and Anson 2006). However, the aggregates used were from the same batch. Therefore, the color change analysis was restricted to the cement paste type (Annerel and Taerwe 2011).

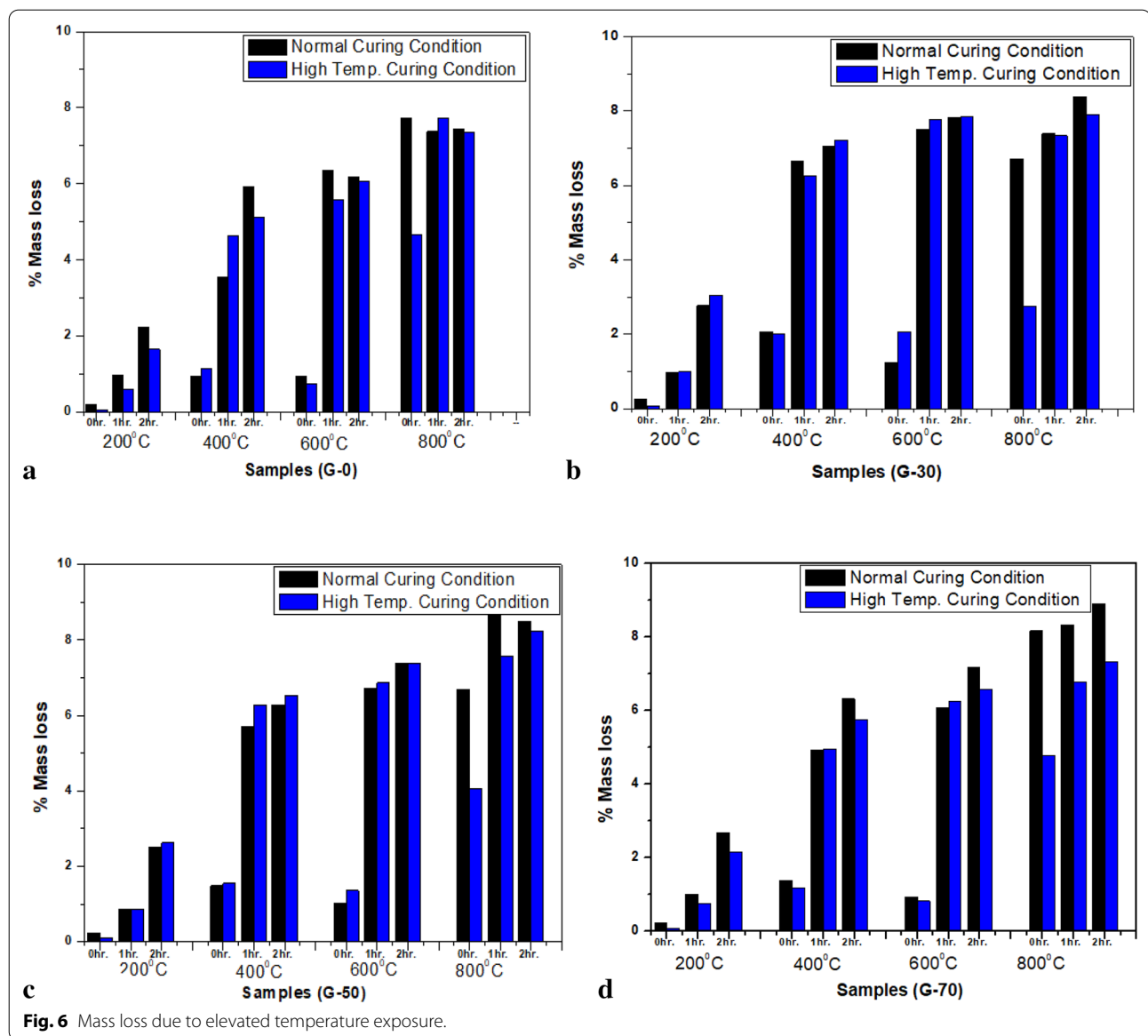


Fig. 6 Mass loss due to elevated temperature exposure.

From visual inspection, the variation in color of the concrete specimens is directly associated with the fire exposure. The color change of the concrete specimens due to fire exposure is irrespective of the curing temperature. The color variations of the concrete specimens post high-temperature fire exposure are summarized in Fig. 7. All concrete specimens exposed to 200 °C for all exposure durations were gray after fire exposure. However, at 400 °C, all concrete specimens exhibited some minor color variations (light gray) in compared with specimens exposed to 200 °C for a 20-min exposure duration. However, when the exposure duration was extended to 140 min, the color of the concrete specimen changed to (old lace = light pink) for concrete groups G-50 and G-70,

whereas the colors of the remaining concrete groups G-0 and G-30 remained unchanged (light gray). A similar color change to light gray in the OPC concrete specimens subjected to fire exposure was observed by (Sarker 2004). As shown in Fig. 7, at 600 °C exposure, all concrete specimens were light gray. However, when the exposure condition was extended for 126 min, concrete group G-0 and G-30 changed to white gray, whereas concrete groups G-50 and G-70 changed to (old lace = light pink). This color change was due to the decomposition of CaCO_3 into CaO and CO_2 under fire exposure. In addition, as reported by (Albrektsson et al. 2011; Kore Sudarshan and Vyas 2019; Shumuye et al. 2019), the presence of iron compounds in fine or coarse aggregates that decomposed

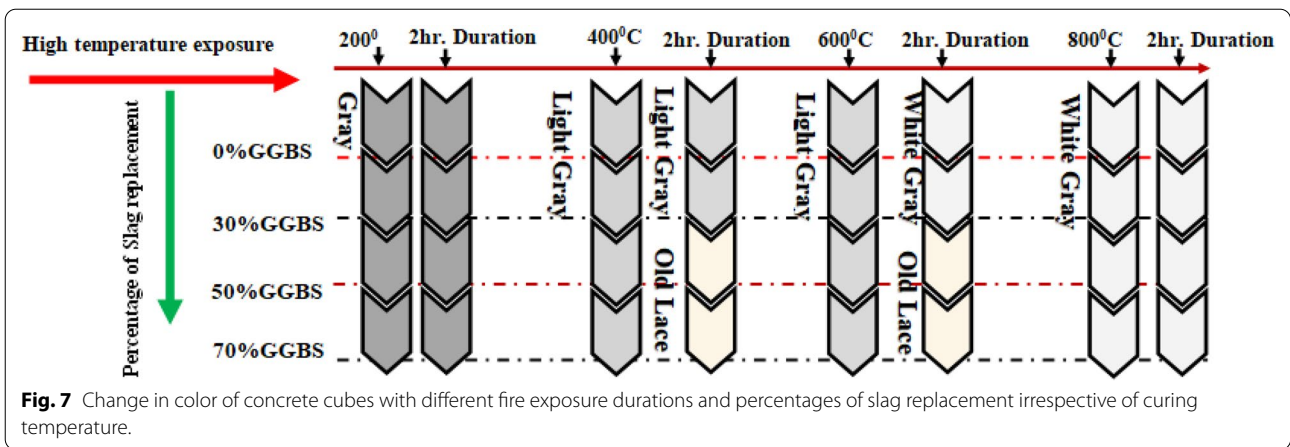


Fig. 7 Change in color of concrete cubes with different fire exposure durations and percentages of slag replacement irrespective of curing temperature.

to its derivatives owing to high temperature resulted in a light pink color.

Owing to the temperature variance between the surface and center of the specimens, surface cracking was prominent in many of the concrete specimens after exposure to fire. As shown in Figs. 8 and 9, the most evident surface cracking was observed in all concrete mix groups when the exposure temperature increased to 800 °C. However, when the exposure temperature increased to 600 °C, a major surface crack was observed for concrete groups

G-0 and G-30, whereas a minor crack was observed for concrete groups G-50 and G-70 for both curing conditions. The surface crack intensity was higher for the concrete groups cured at elevated temperature compared with those cured in the standard curing condition. The surface crack occurred as a result of concrete strain triggered by a temperature gradient through the cross section of the concrete (Sarker 2004). According to (Shumuye et al. 2019), during decarbonation, the additionally formed CaCO_3 expanded its volume by 44%, while

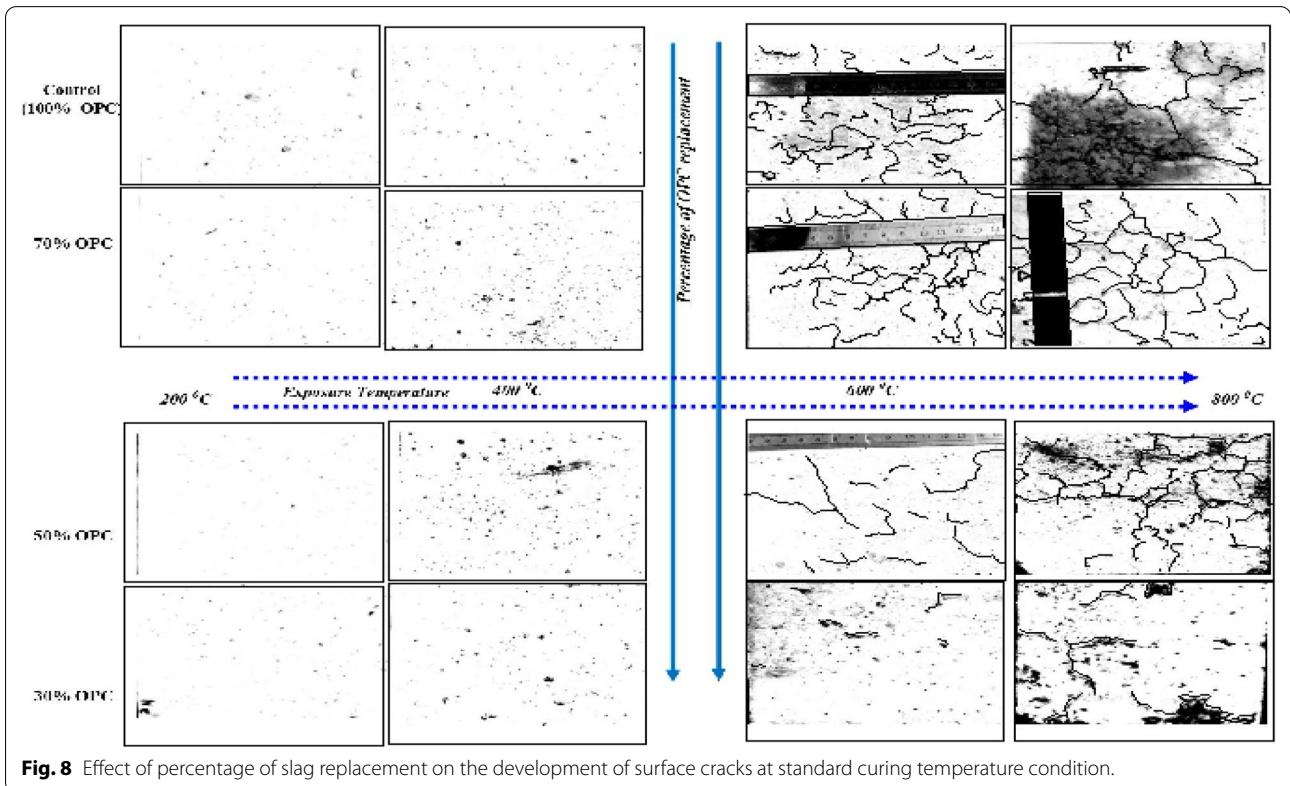


Fig. 8 Effect of percentage of slag replacement on the development of surface cracks at standard curing temperature condition.

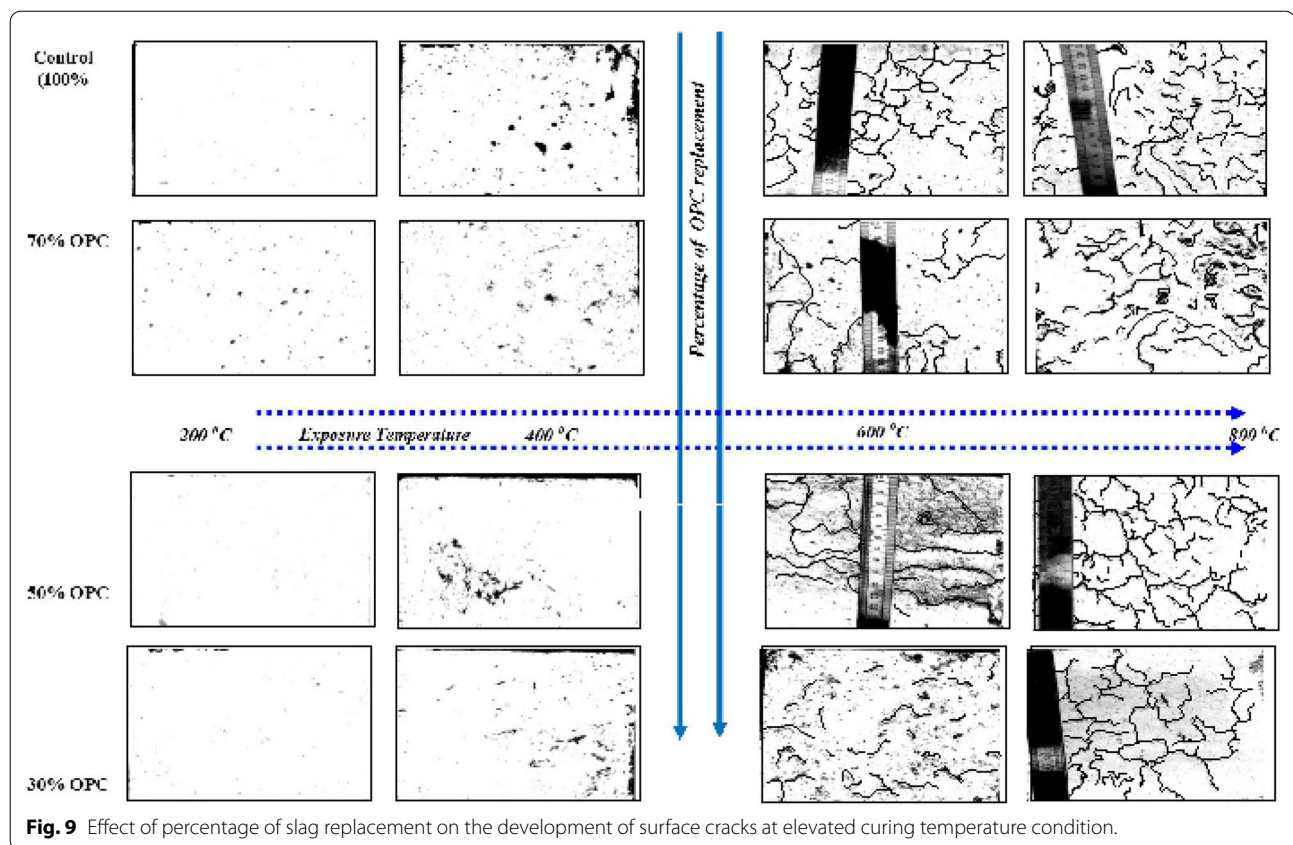


Fig. 9 Effect of percentage of slag replacement on the development of surface cracks at elevated curing temperature condition.

cooling resulted in the formation of cracks and spalling of concrete. Therefore, concrete specimens having a small quantity of CaCO_3 in the cement paste exhibited a minor surface cracking.

The spalling of the concrete specimens at 800 °C is shown in Fig. 10. This type of spalling was observed in all concrete specimens irrespective of the curing temperature and replacement percentage, but the size of spalling for concrete group G-0 was relatively low compared with those of the other concrete specimens. The higher resistance against disintegration and the spalling of concrete group G-0 were due to its intrinsic higher tensile strength and higher CaCO_3 peak compared with those of other concrete mix groups, as shown in Fig. 13.

4.3 XRD

XRD analysis was performed to study the effects of fire exposure and slag replacement level on hydration and phase changes. Figures 11, 12, 13 show a section of the XRD patterns obtained from all concrete groups before and after fire exposure at 400 and 800 °C.

From the XRD data analysis shown in Fig. 12, it was confirmed that after fire exposure, concrete underwent mineralogical changes. One of the major chemical changes was the decomposition of C–S–H gel and

the transformation of $\text{Ca}(\text{OH})_2$ into CaO owing to the exclusion of chemically bonded water. In addition, more peaks appeared for the alpha–beta combination of quartz aggregates after exposure to 800 °C, as shown in Fig. 13. Owing to the decomposition of C–S–H gel and calcium hydroxide, the peaks of the C–S–H gel were lower than those of the unexposed concrete specimens in all concrete mixes. Other major peaks were observed, such as those of SiO_2 , owing to the dissociation of calcium silicate hydrate, as shown in Figs. 11, 12.

The peaks of CaCO_3 and Al_2O_3 for concrete cured in the standard curing condition was relatively low compared to those cured at elevated curing temperature at the early age (7 d). However, at a later age (56 d), the peaks of CaCO_3 and Al_2O_3 were higher for concrete cured at the standard curing condition.

Based on Fig. 12, the reason for the less surface cracking of concrete groups G-50 and G-70 was the less composition of CaCO_3 compared with those of concrete groups G-0 and G-30, which resulted in reduced CO_2 emissions during the decomposition of CaCO_3 at 800 °C exposure.

Therefore, as the slag replacement level increased, the residual amount of CaCO_3 after high-temperature fire exposure decreased. Meanwhile, compared with

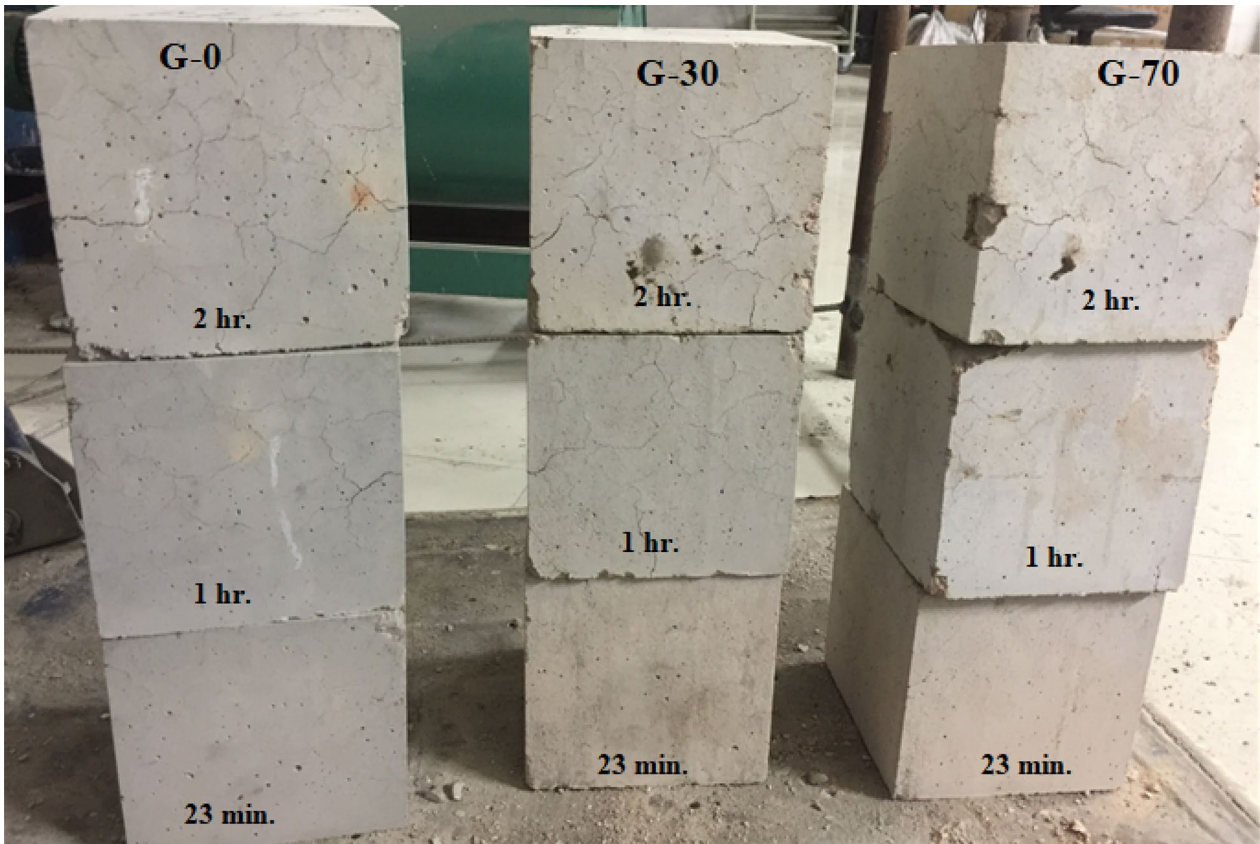


Fig. 10 Cracking and spalling of concrete specimens after 800 °C exposure.

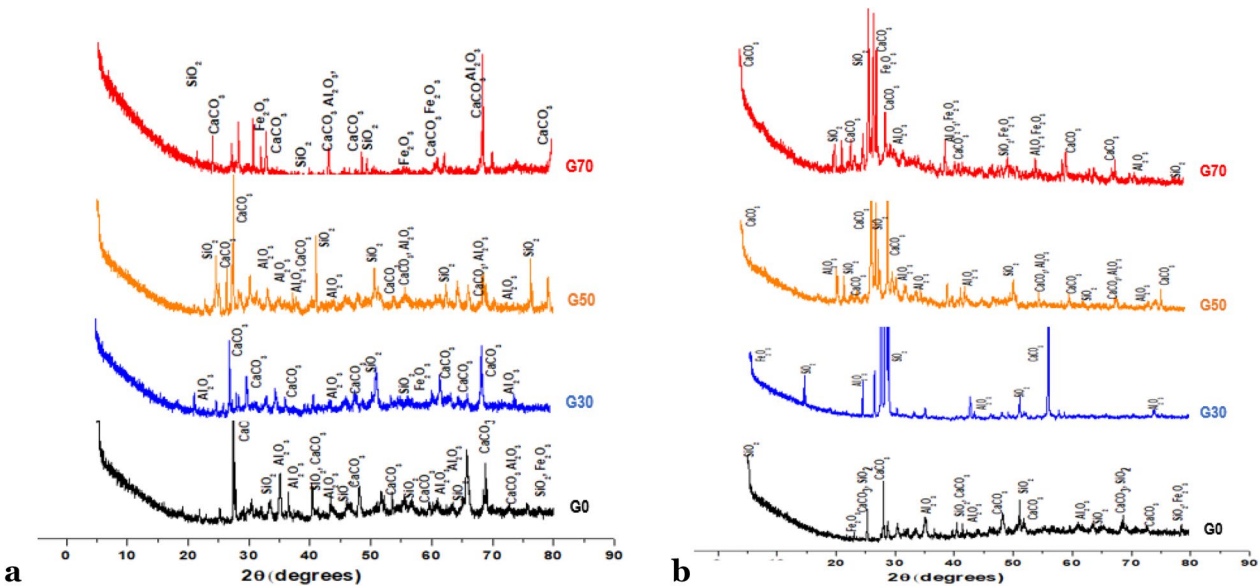
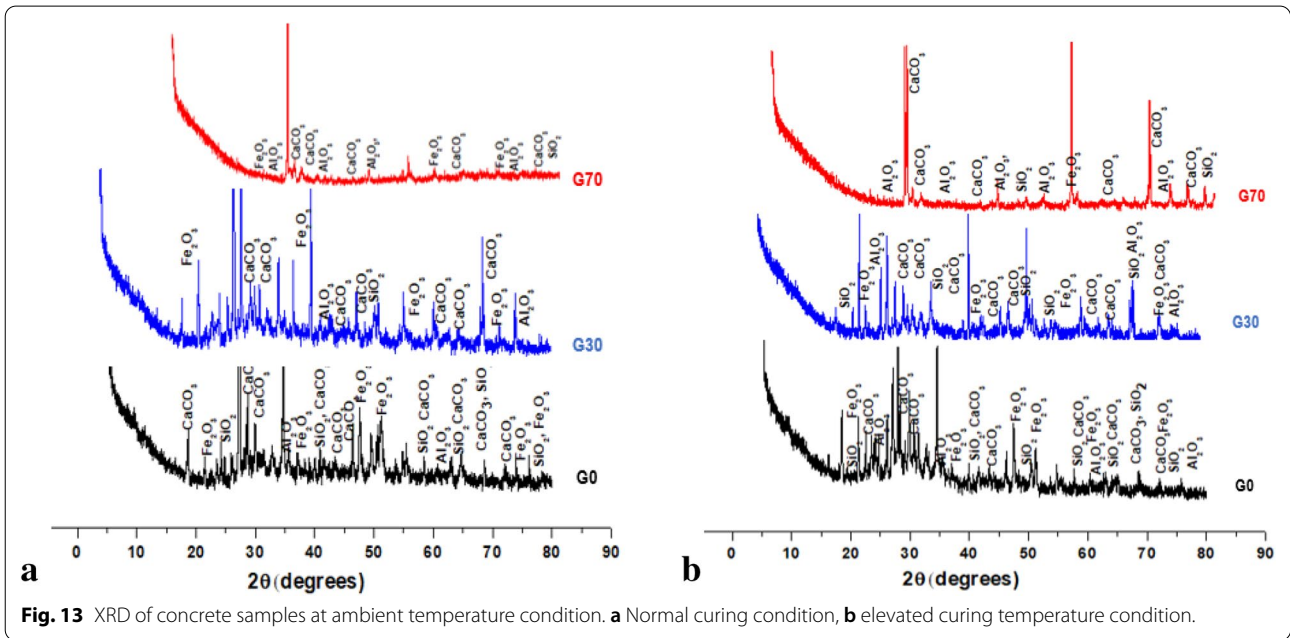
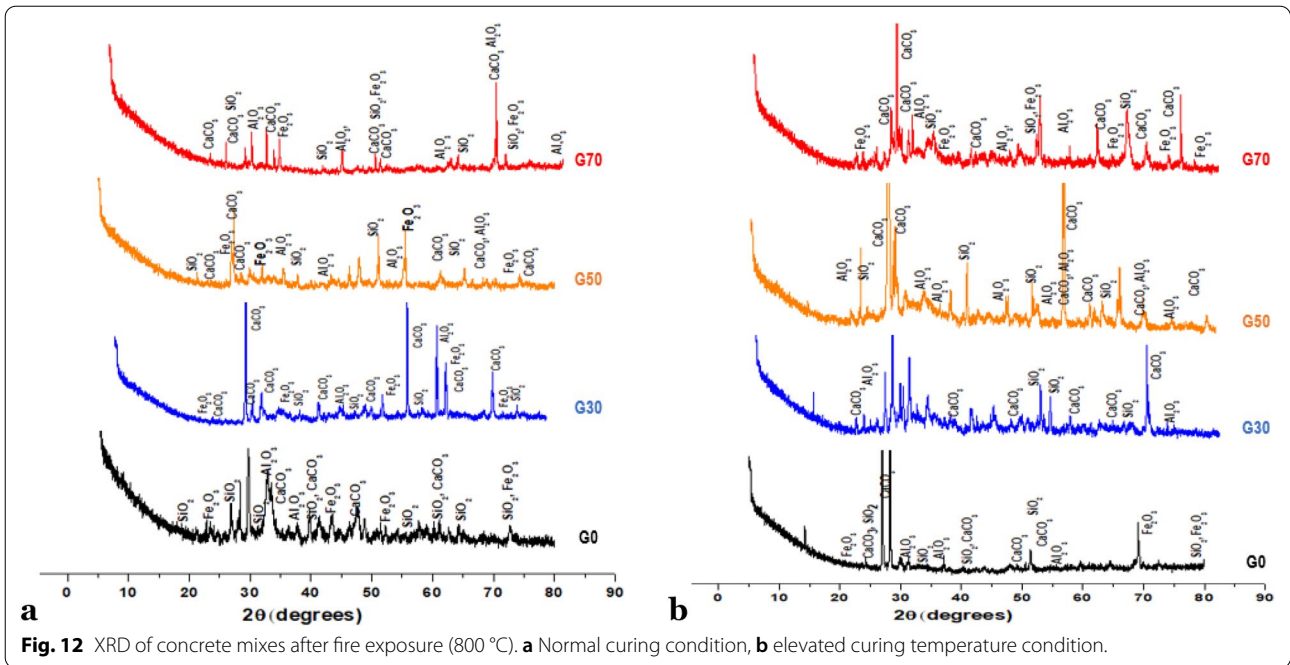


Fig. 11 XRD of concrete mixes after fire exposure (400 °C). **a** Normal curing condition, **b** elevated curing temperature condition.



the other cementitious compounds, the amount of Al_2O_3 increased with the slag replacement level. However, the effect of Al_2O_3 on the compressive strength of the concrete specimens was less compared to that of CaO. The disintegration of $Ca(OH)_2$, $CaCO_3$, and C–S–H resulted in the formation of CaO and $CaSiO_2$. (Kore Sudarshan and Vyas 2019) reported that, owing to decomposition of C–S–H, the loss in mechanical

properties of concrete was significant at 600 and 800 °C fire exposure.

Sharp peaks with various intensity of silicon oxide (SiO_2), calcite ($CaCO_3$), ferrite (Fe_2O_3), quartzite (SiO_2) and aluminate (Al_2O_3) were clearly seen for concrete cured under elevated temperature compared to concrete cured under standard curing condition, exhibiting the presence of good crystallization.

Furthermore, additional peaks were also indicated in the XRD patterns of all concrete samples. As the high-temperature exposure increases from 400 °C to 800 °C, the major peaks shown in Fig. 12 were reduced and leading to poor crystallization of the hydration products. This result agrees with the observed SEM results of the respective concrete. At 800 °C, the intensity of peaks of CaCO_3 (Calcite) shows a remarkable reduction, this might be due to the decomposition of the calcite to CaO and CO_2 . The surprise absence of $\text{Ca}(\text{OH})_2$ was probably caused by the decomposition of portlandite into calcite (Pan et al. 2018; Vyšvařil et al. 2014). Similarly, the silicon oxide phase also indicates reduction due to the gradual decomposition of silicate phases.

4.4 SEM

The microstructure of the concrete specimens provided using different replacement levels of slag subjected to high temperatures were investigated by SEM. Micro-cracks, deterioration in CH and C–S–H phases, and formation of calcium oxide crystals were studied. Even though the microstructure of slag cement concrete has been discussed comprehensively by (Aldea et al. 2000b; Escalante-Garcia and Sharp 2004; Haining and Qiu 2014; Pan et al. 2018; Türker et al. 2016), it is important to study the effect of curing temperature on the microstructural properties of slag cement concrete under fire exposure.

Figure 14 shows the SEM image of 100% OPC concrete and slag cement concrete with 70% and 30% replacement at 7 d for two different curing conditions. It indicated the presence of Portlandite (CH), calcium silicate hydrate (C–S–H), calcium hydroxide ($\text{Ca}(\text{OH})_2$), ettringite

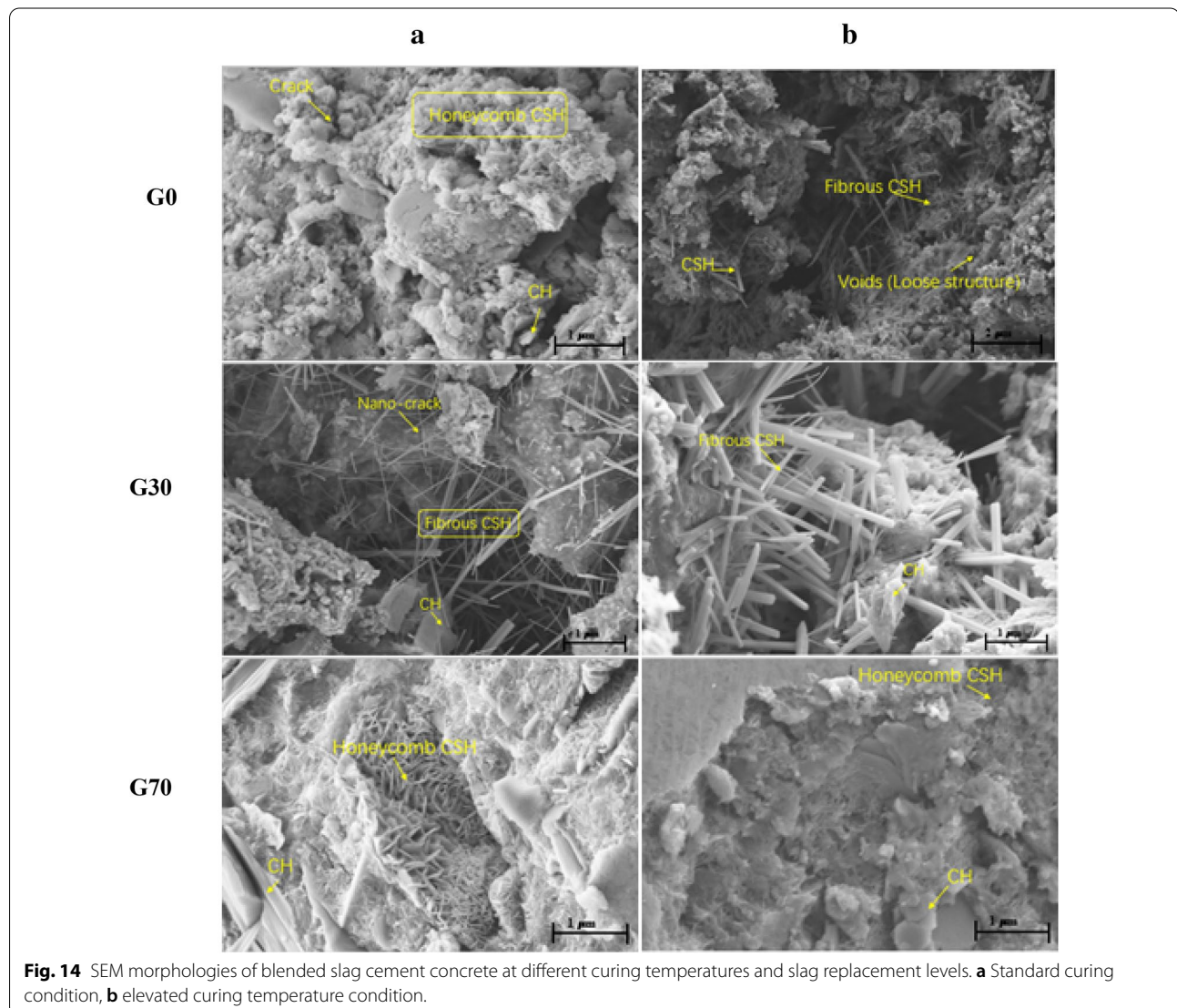


Fig. 14 SEM morphologies of blended slag cement concrete at different curing temperatures and slag replacement levels. **a** Standard curing condition, **b** elevated curing temperature condition.

((Ca₆Al₂(SO₄)₃(OH)). The honeycomb structure of the C–S–H phase, which would continue to solidify and connect with each other, and the CH phase in the form of a thin plate hexagonal crystal have been observed by (Liu et al. 2019).

During hydration, C₃S and C₂S were consumed; consequently, C–S–H and CH phases were created. Concrete groups G-0 and G-30 contained a more condensed amount of C–S–H gel compared to concrete group G-70. From the XRD data for concrete groups G-0 and G-30, the concentration of CaCO₃ was higher compared with that of concrete group G-70. Furthermore, a honeycomb structure of C–S–H phase appeared in concrete group G-70, resulting in the lower compressive strength at the early age compared with concrete groups G-0 and G-30.

The effect of curing temperature was noticeable for all concrete groups. The formation of the C–S–H, CH, and Ca(OH)₂ phases and the presence of ettringite were more prominent for concrete cured at elevated temperature. With the increase in curing temperature, amorphous immature gels were important in linking the ettringite crystalline phase of the hydration product. The density of the crystalline phase was greater for concrete group G-0 compared to concrete group G-70. It can be concluded from Fig. 14 that the microstructure of concrete group G-0 was more homogenous than that of the other concrete groups. Owing to the slag cement, the physical and chemical contributions of the slag cement particles were more prominent for concrete group G-70.

As shown in Figs. 15 and 16, the SEM results for the 28-d curing of the concrete specimens after 400 °C high-temperature fire exposure indicated minor changes in the morphology of all concrete groups compared with the unexposed concrete specimens. The changes were more obvious for concrete groups G-50 and G-70 compared with concrete groups G-0 and G-30. However, when the exposure temperature increased to 800 °C, the predominating amount of micro- and macrocracks, deformation of Ca (OH)₂ crystals, and disintegration of C–S–H phase boundaries were shown in all concrete groups irrespective of the curing temperature. Consequently, a low residual compressive strength was recorded for these concrete groups. A well-hydrated Portland cement paste comprises primarily C–S–H, CH, and ettringite. When the concrete specimens were exposed to high temperatures, the hydrated cementitious products released water gradually to produce a pore pressure in the concrete pore structure.

A few studies have discussed the microstructural properties of slag cement concrete (Campbell 1986; Cho et al. 2017; Fernandes et al. 2017; Pan et al. 2018). Concrete groups G-0 and G-30 exhibited a higher fire endurance compared with the two other concrete groups. Concrete

groups G-0 and G-30 attained the same fire endurance owing to their higher concentrated amounts of calcium silicate hydrate, ettringite, and calcium hydroxide; subsequently, needles of ettringite filled the gap between C–S–H and C–H hydrates, which stabilized the microstructure and hence improved the strength.

5 Conclusion

Concrete produced with supplementary cementitious material (SCM) using GGBS under standard and elevated curing temperature conditions were exposed to fire at 200, 400, 600, and 800 °C, with the temperature increasing at a predetermined rate. Additionally, OPC concrete cubes were exposed to fire using the same heating pattern. The microstructural properties, cracking, spalling, mass loss, splitting tensile strength, and residual compressive strength of OPC and high-volume slag cement concrete under two different curing conditions were compared after high-temperature exposures at different temperatures. The microstructural properties of concrete specimens after high-temperature fire exposure were observed by SEM. Furthermore, the mineralogical composition was analyzed using XRD. The following conclusions were inferred from the test results:

- (1) The effect of curing temperature was noticeable for all concrete groups. The formation of the C–S–H, and Ca(OH)₂ phases and the presence of ettringite were more prominent for concrete cured at elevated temperature than standard curing temperature.
- (2) Concrete specimens cured at elevated temperature exhibited a denser and well-compacted structure compared with concrete specimens cured at the standard curing condition at the early age.
- (3) Concrete groups G-0 and G-30 exhibited a more condensed volume of C–S–H gel compared to concrete group G-70; therefore, a better fire endurance was ensured, and a higher strength development attained.
- (4) The presence of surface cracks was not related to the low strength of the concrete specimens. More surface cracks did not imply a low compressive strength. The surface crack intensity was higher for concrete groups cured at elevated temperature compared with concrete groups cured in the standard curing condition.
- (5) The decrease in residual compressive strength with an increase in high-temperature exposure was significant in the case of concrete cured at elevated temperature, compared with that of specimens cured at the standard curing condition. Furthermore, comparing the two curing conditions, the

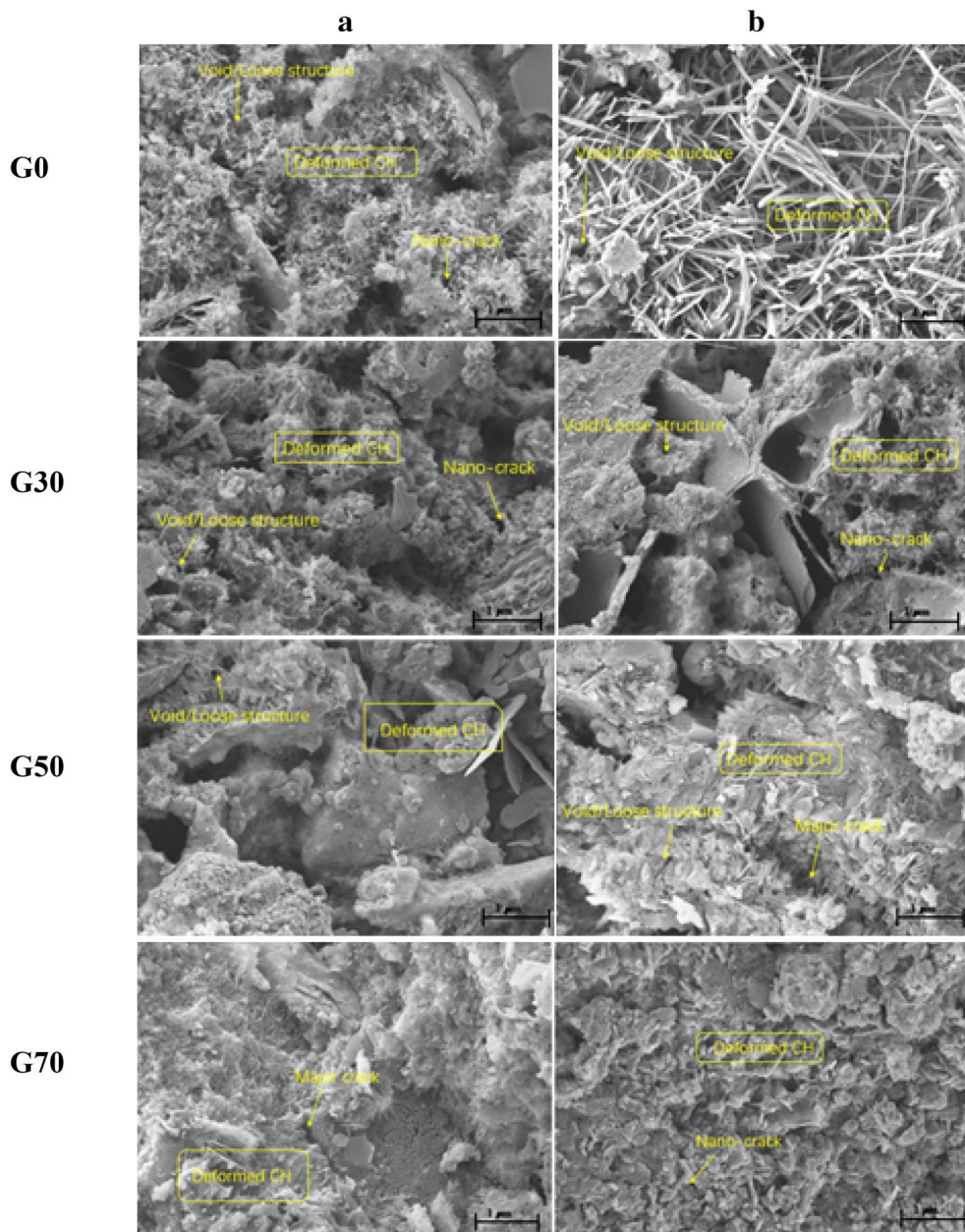


Fig. 15 SEM morphologies of blended slag cement concrete at different curing temperatures and slag replacement levels at 400 °C exposure. **a** Standard curing condition, **b** elevated curing temperature condition.

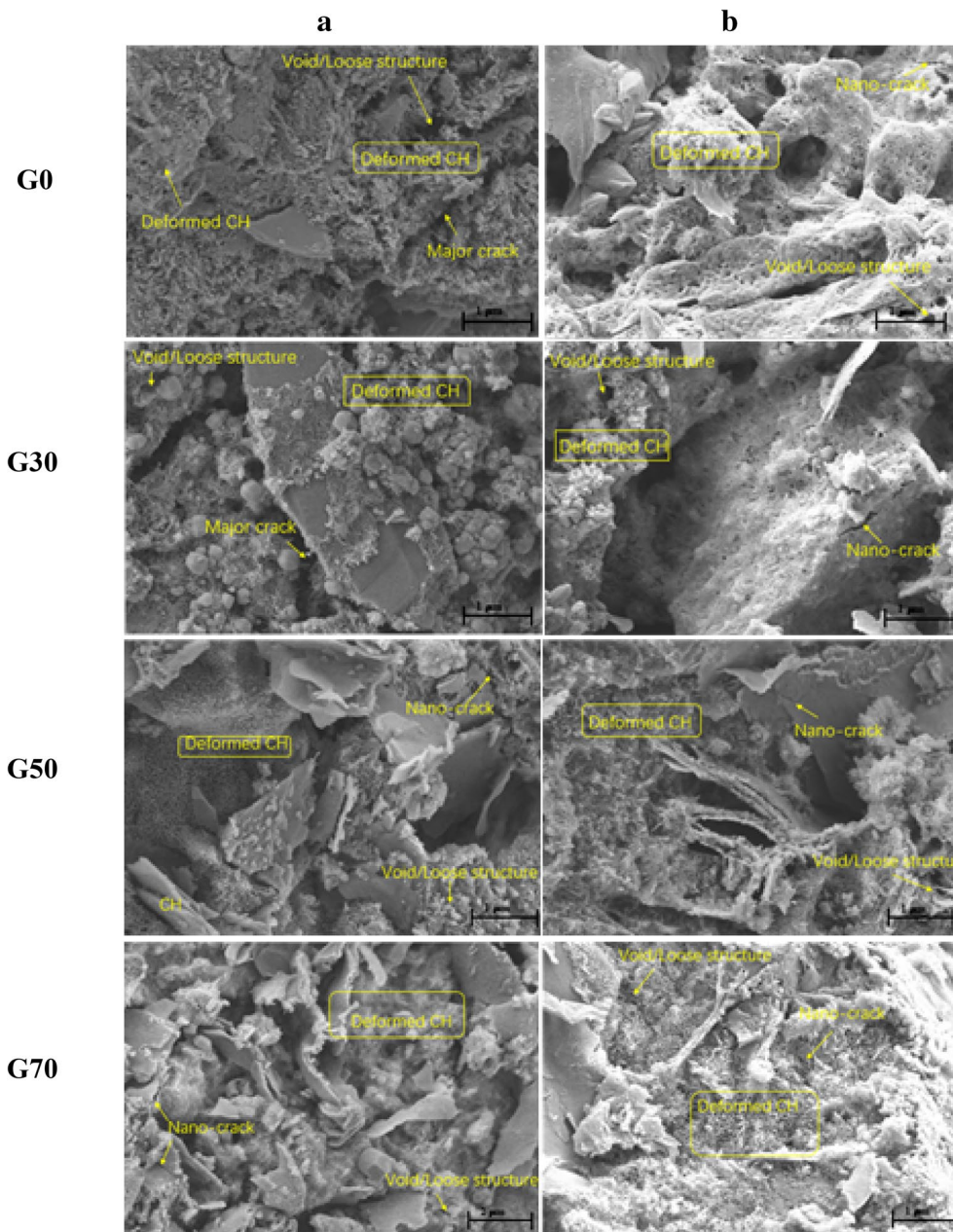


Fig. 16 SEM morphologies of blended slag cement concrete at different curing temperatures and slag replacement levels at 800 °C fire exposure. **a** Standard curing condition, **b** elevated curing temperature condition.

percentage mass loss was more significant for concrete cured at standard curing conditions than that cured at elevated temperature.

Acknowledgements

Experimental work described in this paper was financially supported by Program for Innovative Research Team of Education Ministry of China (IRT_16R67), Thousand Talents Plan in Henan Province (ZYQR201912029), and the National Natural Science Foundation of China (51908512).

Author's informations

JZ is a Professor School of Civil Engineering, Zhengzhou University, Zhengzhou 450001, China.

ZW is a Postdoctoral researcher School of Mechanics and Safety Engineering, Zhengzhou University, Zhengzhou 450001, China.

EDS is a Doctoral student School of Civil Engineering, Zhengzhou University, Zhengzhou 450001, China.

Authors' contributions

All authors contributed substantially to all aspects of this article. All authors read and approved the final manuscript.

Authors' information

Jun Zhao is a Full Professor in School of Civil Engineering at Zhengzhou University, Zhengzhou, Henan, China.

Zike Wang is a postdoctoral researcher in School of Mechanics and Safety Engineering at Zhengzhou University, Zhengzhou, Henan, China.

Eskinder Desta Shumuye is a doctoral student in School of Civil Engineering at Zhengzhou University, Zhengzhou, Henan, China.

Funding

Innovative Research Team of Education Ministry of China, Grant Number: IRT_16R67. Thousand Talents Plan in Henan Province, Grant Number: ZYQR201912029.

Availability of data and materials

The research data used to support the finding of this study are described and included in the article. Furthermore, some of the data used in this study is also supported by providing references as described in the article.

Conflict of interest

The authors declare that they have no conflict of interest.

Author details

¹ School of Civil Engineering, Zhengzhou University, Zhengzhou 450001, China. ² School of Mechanics and Safety Engineering, Zhengzhou University, Zhengzhou 450001, China.

Received: 15 February 2020 Accepted: 8 September 2020

Published online: 23 February 2021

References

- Akca, A. H., & Özyurt, N. (2018). Effects of re-curing on microstructure of concrete after high temperature exposure. *Construction and Building Materials*, 168, 431–441. <https://doi.org/10.1016/j.conbuildmat.2018.02.122>.
- Albrektsson, J., Fla, M., Lindqvist, J. E., & Robert, J. (2011). *Assessment of concrete structures after fire* (No. Brandforsk project number: 301-091). Sweden: SP Sveriges Tekniska Forskningsinstitut.
- Aldea, C.-M., Young, F., Wang, K., & Shah, S. P. (2000a). Effects of curing conditions on properties of concrete using slag replacement. *Cement and Concrete Research*, 30(3), 465–472. [https://doi.org/10.1016/S0008-8846\(00\)00200-3](https://doi.org/10.1016/S0008-8846(00)00200-3).
- Aldea, C.-M., Young, F., Wang, K., & Shah, S. P. (2000b). Effects of curing conditions on properties of concrete using slag replacement. *Cement and Concrete Research*, 30(3), 465–472. [https://doi.org/10.1016/S0008-8846\(00\)00200-3](https://doi.org/10.1016/S0008-8846(00)00200-3).
- Annerel, E., & Taerwe, L. (2011). Methods to quantify the colour development of concrete exposed to fire. *Construction and Building Materials*, 25(10), 3989–3997. <https://doi.org/10.1016/j.conbuildmat.2011.04.033>.
- Arioz, O. (2007). Effects of elevated temperatures on properties of concrete. *Fire Safety Journal*, 42(8), 516–522. <https://doi.org/10.1016/j.firesaf.2007.01.003>.
- ASTM C09 Committee. (2001a). *Practice for making and curing concrete test specimens in the laboratory*. West Conshohocken, PA : ASTM C09 Committee. https://doi.org/10.1520/C0192_C0192M-07.
- ASTM C09 Committee. (2001b). *Test method for splitting tensile strength of cylindrical concrete specimens*. West Conshohocken, PA : ASTM International. https://doi.org/10.1520/C0496_C0496M-04E01.
- ASTM International. (2001). *Standard test method for compressive strength of cylindrical concrete specimens* (No. C 39/C 39M – 01). USA: ASTM International.
- Bakharev, T., Sanjayan, J. G., & Cheng, Y.-B. (1999). Effect of elevated temperature curing on properties of alkali-activated slag concrete. *Cement and Concrete Research*, 29(10), 1619–1625. [https://doi.org/10.1016/S0008-8846\(99\)00143-X](https://doi.org/10.1016/S0008-8846(99)00143-X).
- Barnett, S. J., Soutsos, M. N., Millard, S. G., & Bungey, J. H. (2006). Strength development of mortars containing ground granulated blast-furnace slag: Effect of curing temperature and determination of apparent activation energies. *Cement and Concrete Research*, 36(3), 434–440. <https://doi.org/10.1016/j.cemconres.2005.11.002>.
- Behfarinia, K., & Shahbaz, M. (2018). The effect of elevated temperature on the residual tensile strength and physical properties of the alkali-activated slag concrete. *Journal of Building Engineering*, 20, 442–454. <https://doi.org/10.1016/j.jobbe.2018.08.015>.
- Çakır, Ö., & Aköz, F. (2008). Effect of curing conditions on the mortars with and without GGBFS. *Construction and Building Materials*, 22(3), 308–314. <https://doi.org/10.1016/j.conbuildmat.2006.08.013>.
- Campbell, D. H. (1986). *Microscopical examination and interpretation of Portland cement and clinker*. Skokie, Ill: Construction Technology Laboratories.
- Chan, Y. N., Peng, G. F., & Anson, M. (1999). Residual strength and pore structure of high-strength concrete and normal strength concrete after exposure to high temperatures. *Cement and Concrete Composites*, 21(1), 23–27. [https://doi.org/10.1016/S0958-9465\(98\)00034-1](https://doi.org/10.1016/S0958-9465(98)00034-1).
- China Building Materials Science Research Institute. (2007). *National standard of the people's republic of china*. People's Republic of China: People's Republic of China & Standardization Administration of China.
- Chini, A. R. (2005). Effect of elevated curing temperatures on the strength and durability of concrete. *Materials and Structures*, 38(281), 673–679. <https://doi.org/10.1617/14230>.
- Cho, B. S., Lee, H. H., & Choi, Y. C. (2017). Effects of aluminate rich slag on compressive strength, drying shrinkage and microstructure of blast furnace slag cement. *Construction and Building Materials*, 140, 293–300. <https://doi.org/10.1016/j.conbuildmat.2017.02.111>.
- Durgun, M. Y., & Sevinç, A. H. (2019). High temperature resistance of concretes with GGBFS, waste glass powder, and colemanite ore wastes after different cooling conditions. *Construction and Building Materials*, 196, 66–81. <https://doi.org/10.1016/j.conbuildmat.2018.11.087>.
- El-Yamany, H. E., El-Salamawy, M. A., & El-Assal, N. T. (2018). Microstructure and mechanical properties of alkali-activated slag mortar modified with latex. *Construction and Building Materials*, 191, 32–38. <https://doi.org/10.1016/j.conbuildmat.2018.09.200>.
- Escalante-García, J.-I., & Sharp, J. H. (2004). The chemical composition and microstructure of hydration products in blended cements. *Cement and Concrete Composites*, 26(8), 967–976. <https://doi.org/10.1016/j.cemconcomp.2004.02.036>.
- Fernandes, B., Gil, A. M., Bolina, F. L., & Tutikian, B. F. (2017). Microstructure of concrete subjected to elevated temperatures: Physico-chemical changes and analysis techniques. *Revista IBRACON de Estruturas e Materiais*, 10(4), 838–863. <https://doi.org/10.1590/s1983-41952017000400004>.
- Gencel, O. (2012). Effect of elevated temperatures on mechanical properties of high-strength concrete containing varying proportions of hematite: high-strength concrete containing hematite. *Fire and Materials*, 36(3), 217–230. <https://doi.org/10.1002/fam.1102>.

- Georgali, B., & Tsakiridis, P. E. (2005). Microstructure of fire-damaged concrete. A case study. *Cement and Concrete Composites*, 27(2), 255–259. <https://doi.org/10.1016/j.cemconcomp.2004.02.022>.
- Guerrieri, M., & Sanjayan, J. G. (2009). Behavior of combined fly ash/slag-based geopolymers when exposed to high temperatures. *Fire and Materials*, 34, 163–175. <https://doi.org/10.1002/fam.1014>.
- Haining, G., & Qiu, Li. (2014). Development of microstructure and chemical composition of hydration products of slag activated by ordinary. *Portland cement*. <https://doi.org/10.1016/j.matchar.2013.11.012>.
- ISO 834–1–1999. (1999). *Fire resistance Test-Element of Building Construction*. Part 1: General Requirements, International Organization for Standardization ISO 834, Geneva, Switzerland, 1999.
- Jung, W., & Choi, S.-J. (2017). Effect of high-temperature curing methods on the compressive strength development of concrete containing high volumes of ground granulated blast-furnace slag. *Advances in Materials Science and Engineering*, 2017, 1–6. <https://doi.org/10.1155/2017/7210591>.
- Khan, M. S., Prasad, J., & Abbas, H. (2013). Effect of high temperature on high-volume fly ash concrete. *Arabian Journal for Science and Engineering*, 38(6), 1369–1378. <https://doi.org/10.1007/s13369-013-0606-1>.
- Kim, S. G. (2010). Effect of heat generation from cement hydration on mass concrete placement. Dissertation, Iowa State University. <http://lib.dr.iastate.edu/etd/11675>
- Kore Sudarshan, D., & Vyas, A. K. (2019). Impact of fire on mechanical properties of concrete containing marble waste. *Journal of King Saud University Engineering Sciences*, 31(1), 42–51. <https://doi.org/10.1016/j.jksues.2017.03.007>.
- Lau, A., & Anson, M. (2006). Effect of high temperatures on high performance steel fibre reinforced concrete. *Cement and Concrete Research*, 36(9), 1698–1707. <https://doi.org/10.1016/j.cemconres.2006.03.024>.
- Li, M. Y., & Hu, J. (2014). Influence of high-temperature curing on the properties of the concrete containing ground iron and steel slag. *Applied Mechanics and Materials*, 507, 337–342. <https://doi.org/10.4028/www.scientific.net/AMM.507.337>.
- Liu, J., Yu, Q., Zuo, Z., Yang, F., Han, Z., & Qin, Q. (2019). Reactivity and performance of dry granulation blast furnace slag cement. *Cement and Concrete Composites*, 95, 19–24. <https://doi.org/10.1016/j.cemconcomp.2018.10.008>.
- Long, W.-J., Tan, X.-W., Xiao, B.-X., Han, N.-X., & Xing, F. (2019). Effective use of ground waste expanded perlite as green supplementary cementitious material in eco-friendly alkali activated slag composites. *Journal of Cleaner Production*, 213, 406–414. <https://doi.org/10.1016/j.jclepro.2018.12.118>.
- Lublóy, É., Kopeckó, K., Balázs, G. L., Restás, Á., & Szilágyi, I. M. (2017). Improved fire resistance by using Portland-pozzolana or Portland-fly ash cements. *Journal of Thermal Analysis and Calorimetry*, 129(2), 925–936. <https://doi.org/10.1007/s10973-017-6245-0>.
- Mendes, A., Sanjayan, J. G., & Collins, F. (2009). Long-term progressive deterioration following fire exposure of OPC versus slag blended cement pastes. *Materials and Structures*, 42(1), 95–101. <https://doi.org/10.1617/s11527-008-9369-7>.
- Mohammadhosseini, H., Lim, N. H. A. S., Sam, A. R. M., & Samadi, M. (2018). Effects of elevated temperatures on residual properties of concrete reinforced with waste polypropylene carpet fibres. *Arabian Journal for Science and Engineering*, 43(4), 1673–1686. <https://doi.org/10.1007/s13369-017-2681-1>.
- Netinger, I., Varevac, D., Bjegović, D., & Morić, D. (2013). Effect of high temperature on properties of steel slag aggregate concrete. *Fire Safety Journal*, 59, 1–7. <https://doi.org/10.1016/j.firesaf.2013.03.008>.
- Pan, Z., Tao, Z., Cao, Y. F., Wuhrer, R., & Murphy, T. (2018). Compressive strength and microstructure of alkali-activated fly ash/slag binders at high temperature. *Cement and Concrete Composites*, 86, 9–18. <https://doi.org/10.1016/j.cemconcomp.2017.09.011>.
- RILEM Technical Committee 200-HTC. (2007a). Recommendation of RILEM TC 200-HTC: Mechanical concrete properties at high temperatures—modelling and applications: Part 1: Introduction—General presentation. *Materials and Structures*, 40(9), 841–853. <https://doi.org/10.1617/s11527-007-9285-2>.
- RILEM Technical Committee 200-HTC. (2007b). Recommendation of RILEM TC 200-HTC: Mechanical concrete properties at high temperatures—modelling and applications: Part 2: Stress–strain relation. *Materials and Structures*, 40(9), 855–864. <https://doi.org/10.1617/s11527-007-9286-1>.
- Sarker, P. K. (2014). Effect of fire exposure on cracking, spalling and residual strength of fly ash geopolymer concrete. *Materials and Design*. <https://doi.org/10.1016/j.matdes.2014.06.059>.
- Shumuye, E. D., Zhao, J., & Wang, Z. (2019). Effect of fire exposure on physico-mechanical and microstructural properties of concrete containing high volume slag cement. *Construction and Building Materials*, 213, 447–458. <https://doi.org/10.1016/j.conbuildmat.2019.04.079>.
- Tang, Y., Su, H., Huang, S., Qu, C., & Yang, J. (2017). Effect of curing temperature on the durability of concrete under highly geothermal environment. *Advances in Materials Science and Engineering*, 2017, 1–9. <https://doi.org/10.1155/2017/7587853>.
- Türker, H. T., Balçikanlı, M., Durmuş, İH., Özbay, E., & Erdemir, M. (2016). Microstructural alteration of alkali activated slag mortars depend on exposed high temperature level. *Construction and Building Materials*, 104, 169–180. <https://doi.org/10.1016/j.conbuildmat.2015.12.070>.
- Ukpata, J. O., Basheer, P. A. M., & Black, L. (2019). Slag hydration and chloride binding in slag cements exposed to a combined chloride-sulphate solution. *Construction and Building Materials*, 195, 238–248. <https://doi.org/10.1016/j.conbuildmat.2018.11.055>.
- Vieira, J. P. B., Correia, J. R., & de Brito, J. (2011). Post-fire residual mechanical properties of concrete made with recycled concrete coarse aggregates. *Cement and Concrete Research*, 41(5), 533–541. <https://doi.org/10.1016/j.cemconres.2011.02.002>.
- Vyšvařil, M., Bayer, P., Chromá, M., & Rovnaníková, P. (2014). Physico-mechanical and microstructural properties of rehydrated blended cement pastes. *Construction and Building Materials*, 54, 413–420. <https://doi.org/10.1016/j.conbuildmat.2013.12.021>.
- Wang, H. Y. (2008). The effects of elevated temperature on cement paste containing GGBFS. *Cement and Concrete Composites*, 30(10), 992–999. <https://doi.org/10.1016/j.cemconcomp.2007.12.003>.
- Wang, Q., Li, M., & Jiang, G. (2014). The difference among the effects of high-temperature curing on the early hydration properties of different cementitious systems. *Journal of Thermal Analysis and Calorimetry*, 118(1), 51–58. <https://doi.org/10.1007/s10973-014-3979-9>.
- Yang, H., Zhao, H., & Liu, F. (2018). Residual cube strength of coarse RCA concrete after exposure to elevated temperatures. *Fire and Materials*, 42(4), 424–435. <https://doi.org/10.1002/fam.2508>.
- Yermak, N., Pliya, P., Beaucour, A.-L., Simon, A., & Noumowé, A. (2017). Influence of steel and/or polypropylene fibres on the behaviour of concrete at high temperature: Spalling, transfer and mechanical properties. *Construction and Building Materials*, 132, 240–250. <https://doi.org/10.1016/j.conbuildmat.2016.11.120>.
- Yu, K.-Q., Dai, J.-G., Lu, Z.-D., & Leung, C. K. Y. (2015). Mechanical properties of engineered cementitious composites subjected to elevated temperatures. *Journal of Materials in Civil Engineering*, 27(10), 04014268. [https://doi.org/10.1061/\(ASCE\)MT.1943-5533.0001241](https://doi.org/10.1061/(ASCE)MT.1943-5533.0001241).
- Zhang, B., Bicanic, N., Pearce, C. J., & Balabanic, G. (2000). Residual fracture properties of normal- and high-strength concrete subject to elevated temperatures. *Magazine of Concrete Research*, 2, 14.
- Zhao, H., Wang, Y., & Liu, F. (2017). Stress–strain relationship of coarse RCA concrete exposed to elevated temperatures. *Magazine of Concrete Research*, 69(13), 649–664. <https://doi.org/10.1680/jmacr.16.00333>.

Publisher's Note

Springer Nature remains neutral with regard to jurisdictional claims in published maps and institutional affiliations.

Submit your manuscript to a SpringerOpen® journal and benefit from:

- Convenient online submission
- Rigorous peer review
- Open access: articles freely available online
- High visibility within the field
- Retaining the copyright to your article

Submit your next manuscript at ► [springeropen.com](https://www.springeropen.com)